HHS Public Access

Author manuscript

J Mater Chem B. Author manuscript; available in PMC 2019 April 21.

Published in final edited form as:

J Mater Chem B. 2018 April 21; 6(15): 2204–2216. doi:10.1039/C7TB03106H.

The in vivo fates of plant viral nanoparticles camouflaged using self-proteins: overcoming immune recognition

N. M. Gulati[‡,a,b], **A. S. Pitek**[‡,c], **A. E. Czapar**[c], **P. L. Stewart**[*,a,b], and **N. F. Steinmetz**[*,c,d,e,f,g]

[a]Department of Pharmacology, Case Western Reserve University, Cleveland, Ohio

[b]Cleveland Center for Membrane and Structural Biology, Case Western Reserve University, Cleveland, Ohio

[c]Department of Biomedical Engineering, Case Western Reserve University, Cleveland, Ohio

[d]Department of Radiology, Case Western Reserve University, Cleveland, Ohio

[e]Department of Materials Science and Engineering, Case Western Reserve University, Cleveland, Ohio

[f]Department of Macromolecular Science and Engineering, Case Western Reserve University, Cleveland, Ohio

[g]Case Comprehensive Cancer Center, Division of General Medical Sciences-Oncology, Case Western Reserve University, Cleveland, Ohio

Abstract

Nanoparticles offer a promising avenue for targeted delivery of therapies. To slow clearance, nanoparticles are frequently stealth-coated to prevent opsonization and immune recognition. Serum albumin (SA) has been used as a bio-inspired stealth coating. To develop this shielding strategy for clinical applications, it is critical to understand the interactions between the immune system and SA-camouflaged nanoparticles. This work investigates the in vivo processing of SA-coated nanoparticles using tobacco mosaic virus (TMV) as a model system. In comparing four different SA-formulations, the particles with high SA coverage conjugated to TMV via a short linker performed the best at preventing antibody recognition. Irrelevant of the coating chemistry, all formulations led to similar levels of TMV-specific antibodies after repeat administration in mice; importantly though, SA-specific antibodies were not detected and the TMV-specific antibodies were unable to recognize shielded SA-coated TMV. Upon uptake in macrophages, the shielding agent and nanoparticle separate, where TMV trafficked to the lysosome and SA appears to recycle. The distinct intracellular fates of the TMV carrier and SA shielding agent explain why anti-TMV but not SA-specific antibodies are generated. This work characterizes the outcomes of SA-camouflaged TMV after immune recognition, and highlights the effectiveness of SA as a nanoparticle shielding agent.

[*]Corresponding Authors: Nicole F. Steinmetz, Ph.D.; nicole.steinmetz@case.edu; Phone: 216-368-4377; Fax: 216-844-4987 and Phoebe L. Stewart, Ph.D.; pls47@case.edu; Phone: 216-368-4349; Fax: 216-368-1300.
[‡]These authors contributed equally to this work.

Conflicts of interest: There are no conflicts to declare.

Graphical abstract

Nanoparticle camouflage with serum albumin is formulation specific, does not produce antibodies against the coating, and shields nanoparticle antibody recognition.

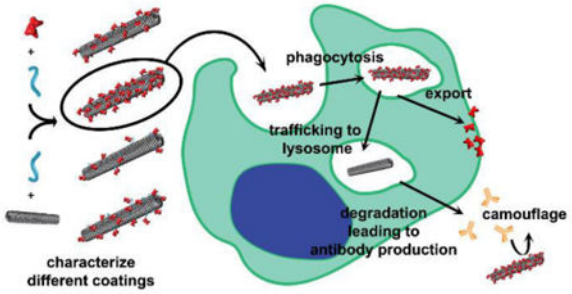

Introduction

Nanoparticle-based delivery platforms have shown success in delivery of therapeutic molecules to disease sites while limiting off-target side effects. Yet despite the success of Doxil® (PEGylated liposomal doxorubicin) and other clinically-approved nanoparticle formulations, barriers remain in the development of these therapies. For a nanoparticle to successfully reach target tissue and deliver its payload, it first must encounter and overcome the host's defenses: the immune system.[1] Nanoparticles can be recognized by complement or other innate immune proteins as well as neutralizing antibodies, which can adsorb to the surface of the nanoparticle to create a protein ‘corona’ and direct them for clearance through the mononuclear phagocyte system, preventing them from ever reaching target tissue.[2-4] This clearance can be reduced by coating nanoparticles with shielding agents to create ‘stealth’ or ‘camouflage’ effects and thus overcome immune clearance.

The most common approach is to ‘stealth’ nanoparticles through polyethylene glycol (PEG) coatings. This hydrophilic coating reduces nanoparticle-protein interactions and thus reduces protein corona formation, immune recognition, and premature clearance. However, PEGs come in different shapes and sizes, and the effectiveness of shielding is dependent on the specific PEG polymer chosen – there is no ‘one-fits-all’ solution and each PEGylated nanoparticle system needs to be carefully optimized.[5-7] Furthermore, with the prevalence of PEG in commercial products, there has been an increase in PEG-specific antibodies found in the human population.[8, 9] These antibodies limit the effectiveness of the polymer shield, especially upon repeat administrations of a treatment.[10, 11] Newer strategies include alternate polymers as well as the use of ‘self’ coatings as stealth agents.

One avenue is to camouflage nanoparticles by coating them with ‘self’ molecules, including proteins and lipids, among others. It has been shown that using a ‘self’ minimal peptide of CD47 prevented nanoparticle clearance by the mononuclear phagocyte system by acting as an ‘eat me not’ signal.[12] Nanoparticles formulated with self-coatings have been shown to exhibit longer circulation times and decreased immune recognition compared to PEGylated nanoparticles.[12-14] This highlights the potential of these ‘self’ coatings as nanoparticle shielding agents.

Recently, our lab published results demonstrating the benefits of using serum albumin (SA) as a 'self' protein camouflage.[13] SA, which functions to transport hydrophobic molecules in the blood, is the most abundant protein in plasma, making it an ideal candidate for 'self' camouflage. As a nanocarrier platform, we used tobacco mosaic virus (TMV). The nucleoprotein components of TMV form a 300 nm × 18 nm rigid rod made up of 2130 identical coat proteins. The virus architecture is stable in plasma, and modifications can be made to the interior and exterior of the virus for nanotechnology applications.[15-17] The TMV platform has been studied for drug delivery and imaging applications.[18-20] Tobacco mosaic virus and other plant viral nanoparticles are noninfectious in humans, making it a suitable candidate for therapeutic applications. However, like other proteinaceous nanoparticles, naked TMV has a short half-life (3.5 minutes) in naïve mice.[15] Moreover, anti-TMV antibodies can be found in human serum of both smokers and nonsmokers due to the presence of TMV in tobacco and food products.[21-27] Therefore, it is imperative that an effective stealth technology is applied for TMV-based contrast agents and therapeutic drug delivery.

We have shown that compared to their PEGylated counterparts, SA-TMV nanoparticles had reduced antibody recognition and longer circulating half-lives.[13] Structural characterization of SA-camouflaged TMV indicated dense coverage of SA on the TMV surface and random orientations of SA with respect to the TMV coat proteins (CPs).[28] Here, we set out to characterize the SA-coated TMV nanoparticle system further and to gain insight into the structure-function relationship of SA coatings, displayed at distinct density and conjugated via short vs. long PEG linkers. We elucidate immune recognition and intracellular processing pathways of SA-coated TMV nanoparticles using a combination of tissue culture, *in vivo* and *ex vivo* assays.

Experimental

Materials and Methods

Virus propagation and purification—Tobacco mosaic virus or its T158K mutant (TMV-lys)[17] was propagated by mechanical inoculation using 5-10 μg virus per leaf. Viruses were isolated and purified as previously described[16] to yield approximately 1 mg virus / 1 g infected leaf material.

TMV sCy5 labeling—TMV particles were internally labeled at glutamic acid residues with sCy5 fluorescent dyes. First, glutamic acids were modified using EDC coupling with alkynes using 1 mg/mL TMV, 100 equivalents of propargylamine (Sigma-Aldrich) per capsid protein, and 50 equivalents EDC (25 equivalents added at 0 and 16 hours) in 100 mM HEPES buffer, pH 7.4 reacted for 20 hours at RT. Alkyne-azide click chemistry was then performed using 1.5 equivalent of sCy5-azide (Lumiprobe) per coat protein with 2 mg/mL TMV in the presence of 1 mM $CuSO_4$ (Fisher), 2 mM AMG (Fisher), 2 mM AsC (Fisher) in 10 mM potassium phosphate buffer, pH 7.5 on ice for 30 min. TMV was purified by ultracentrifugation at 42,000 rpm for 3 hours on a 40% (w/v) sucrose cushion in 10 mM potassium phosphate buffer, pH 7.5.

TMV external conjugation—Human or mouse SA (Sigma-Aldrich or Bioworld respectively) was externally conjugated to TMV-lys using combination of intermediate PEG linkers in multistep reaction. First, SA was conjugated with NHS-PEG_4-SAT (ThermoFisher) at 1:1 ratio in phosphate buffered saline (PBS; 0.01 M Na_2HPO_4, 0.0018 M KH_2PO_4, 0.0027 M KCl and 0.137 M NaCl, pH 7.4) containing 10% (v/v) DMSO overnight at RT. To de-protect the thiol group, 0.5 M hydroxylamine, 25 mM EDTA in PBS, pH 7.2-7.5 was added at a final concentration of 10% (v/v) and incubated for 2 hours at RT. Separately, TMV-lys was conjugated with maleimide-PEG_4-NHS (ThermoFisher) or maleimide-PEG_{24}-NHS (ThermoFisher) at 10 (for high coverage particles) or 3 (for low coverage particles) equivalents of PEG per coat protein in 10 mM potassium phosphate buffer, pH 7.4 containing 10% (v/v) DMSO for 2 hours at RT. The resulting maleimide-PEG-TMV conjugates were purified twice through PD MiniTrap G-25 desalting columns (GE) and divided into two aliquots: a) control PEG-TMV nanoparticles used in dot blot experiments, and b) PEG-TMV nanoparticles subsequently combined with previously prepared SA-PEG-SH at 6 (for high coverage particles) or 2 (for low coverage particles) equivalents per CP, and reacted overnight at RT to yield SA-$PEG_{8/28}$-TMV particles of variable SA coverage. Both a) and b) were quenched by addition of excess glycine and L-cysteine for 1 hour at RT. The resulting constructs were then purified by ultracentrifugation at 55,000 rpm for 3 hours on a 40% (w/v) sucrose cushion.

SDS-PAGE analysis—Samples were denatured by boiling at 100°C for 5 minutes in gel loading buffer (62.5 mM Tris H Cl pH 6.8, 2% w/v SDS, 10% v/v glycerol, 0.01 % w/v bromophenol blue, 10% v/v 2-β-mercaptoethanol). 20 μg TMV was loaded on 4-12% Bis/Tris NuPAGE gels (ThermoFisher Scientific) and separated at 200 V for 35 minutes in MOPS running buffer. When fluorescent particles were used, the sCy5-labelled TMV CP bands were detected using a Maestro fluorescence imaging system. Subsequently, the gels were stained using Coomassie Blue, visualized using an AlphaImager imaging system (Biosciences) and underwent densitometry analysis using ImageJ software.[29]

Western blot analysis—Samples prepared by SDS-PAGE as described above were transferred to nitrocellulose membranes at 30 V for 1 hour. Membranes were blocked with 5% (w/v) milk in TBS-Tween (150 mM NaCl, 10 mM Tris HCl, 0.1% (v/v) Tween-20, pH 7.5) for 1 hour at RT. Membranes were then incubated with 0.5 μg/mL rabbit polyclonal anti-TMV antibody (custom-made, Pacific Immunology) or rabbit polyclonal anti-albumin antibody (NBP1-32458, Novus Biologicals) in 5% (w/v) milk in TBS-Tween overnight at 4°C. Membranes were then washed three times for 10 min each in TBS-Tween, followed by incubation with 1 μg/mL alkaline phosphatase-conjugated goat anti-rabbit antibody (G21079, Thermo Fisher Scientific) in 5% (w/v) milk in TBS-Tween for 1 hour at RT, followed by three washes for 10 min each in TBS-Tween and one 5 min wash in dH_2O. Antibody binding was visualized using Novex AP Chromogenic Substrate (BCIP/NBT; Invitrogen).

Negative stain transmission electron microscopy—3 μL sample at a concentration of 0.5 mg/mL was applied to glow-discharged carbon coated 200 mesh copper grids. After 1 minute, excess sample was removed. Grids were then washed two times in dH_2O for 1

minute each, then stained two times for 30 seconds each with 2% (w/v) uranyl acetate. Grids were then blotted until dry with Whatman 1 blotting paper. All grids were imaged on a JEOL 2200FS 200 kV transmission electron microscope equipped with an energy filter using a Tietz TVIPS 4k × 4k CMOS camera.

Dot blots—Blots were prepared by spotting 1 μL of 150 μg/mL rabbit polyclonal anti-TMV antibody (custom-made, Pacific Immunology), rabbit polyclonal anti-CPMV antibody (custom-made, Pacific Immunology), rabbit monoclonal anti-PEG antibody (AB133471, Abcam), or 1:200 diluted mouse plasma on a nitrocellulose membrane, after the nitrocellulose membrane was equilibrated in PBS. Blots were incubated in 5% (w/v) milk in PBS at RT for 1 hour, then washed three times for 5 minutes each in PBS. Blots were then incubated with 40 μg/mL fluorescently-labeled particles for 2.5 hours at RT, then washed three times for 5 minutes each in PBS. Blots were dried and imaged using a Maestro imaging system. Blots were analyzed using ImageJ. Blots shown together within a single figure panel were imaged simultaneously to limit differences that may occur because of the camera setup.

In vivo studies and ELISA assays—Animals were housed, bred, and handled in the Case Western Reserve University Animal Resource Center in accordance with experimental protocols approved by the Case Western Reserve University Institutional Animal Care and Use Committee. Balb/C mice were injected via tail vein with 200 μg SA-TMV constructs or TMV or SA + TMV on days 0, 7, 14, 21, and 28. Blood was collected retro-orbitally in heparin-coated tubes (ThermoFisher Scientific) on days 0, 14, 28 prior to injection, and on day 56. Plasma was separated by centrifugation at 2000 rcf for 10 min, then stored at -20°C until analysis.

TMV-specific and SA-specific plasma IgG antibodies were determined by ELISA analysis. 96-well Nunc Polysorb Immuno Plates (ThermoFisher Scientific) were coated with 1 μg SA or TMV/well in coating buffer (0.05 M Na_2CO_3, 0.05 M $NaHCO_3$, 0.015 M NaN_3 in dH_2O, pH 9.6) and incubated overnight at 4°C. After coating, wells were blocked with blocking buffer (2.5% (w/v) milk, 25% FBS in PBS, pH 7.4) at 37°C for 1 hr, followed by four washes with washing buffer (0.1% Tween-2 in PBS, pH 7.4). 100 μL of serially diluted plasma (1:200, 1:500, 1:1000, or 1:5000) in blocking buffer was then added to each well and incubated at 37°C for 2 hr. Wells were then washed five times with washing buffer, followed by the addition of 100 μL alkaline phosphate-labeled goat anti-mouse IgG (Life Technologies at 1:3000 in blocking buffer and incubated at 37°C for 1 hr. Wells were then washed five times with washing buffer, then developed by adding 100 μL one-step PNPP substrate (ThermoFisher Scientific) for 10 min at 4°C. The reactions were stopped by addition of 100 μL 2 M NaOH and absorbance was measured at 405 nm using a Tecan Infinity 200 microplate reader.

Confocal microscopy—Confluent RAW 264.7 murine macrophage cells were cultured in DMEM (Corning) containing 10% (v/v) fetal bovine serum and 1% (v/v) penicillin/streptomycin at 37°C and 5% CO_2. Confluent cells were removed using 0.05% (w/v) trypsin-EDTA (Corning) and cultured to glass coverslips in 24-well untreated plates at 20,000 cells/well overnight. Cells were incubated for 6, 12, 24 hr, or 12 hr followed by wash

and incubation with media for 12 hr. Following incubation, cells were fixed in DPBS containing 5% (v/v) paraformaldehyde and 0.3% (v/v) glutaraldehyde for 10 min at room temperature. After fixation, cells were permeabilized with 0.2% Triton-X 100 for 2 min followed by blocking in 5% (v/v) goat serum, 0.5% (v/v) Fc block in DPBS for 45 min at room temperature. Cells were then stained with 1:200 diluted primary antibodies in 5% (v/v) goat serum, 0.5% (v/v) Fc block in DPBS for 1 hr at room temperature and 1:1000 diluted secondary antibodies in 5% (v/v) goat serum, 0.5% (v/v) Fc block in DPBS for 1 hr at room temperature. Lysosomes were stained using goat anti-mouse LAMP-1 conjugated to AlexaFluor 488 (328609; BioLegend). TMV was stained using rabbit anti-TMV primary antibody and AlexaFluor 647-conjugated goat anti-rabbit secondary antibody (A-21244; ThermoFisher Scientific). SA was stained using chicken anti-SA primary antibody (AB106582, Abcam) and AlexaFluor 555-conjugated goat anti-chicken secondary antibody (AB150174, Abcam). Cells were washed three times with DPBS (Corning) between steps. Coverslips were mounted onto slides using Fluoroshield with DAPI (Sigma-Aldrich). Slides were imaged using a Leica TCS SPE confocal laser scanning microscope and the data were processed with ImageJ.

Lysosomal extraction experiments—Animals were housed, bred, and handled in the Case Western Reserve University Animal Resource Center in accordance with approved Institutional Animal Care and Use Committee experimental protocols. Female FVB mice were starved overnight and euthanized using carbon dioxide inhalation. Livers were removed and lysosomes were extracted from them using the Lysosome Isolation Kit (Sigma-Aldrich), based on the protocol provided with the kit, however no protease inhibitors were used. Following lysosomal extraction, the presence of lysosomal enzymes was determined using the Acid Phosphatase Kit (Sigma-Aldrich). Lysosomal extract was then incubated with bovine serum albumin (BSA) as an internal control to determine enzymatic activity of lysosomal proteases, as lysosomal extract has been shown previously to degrade BSA.[30] After confirming enzymatic activity, Cy5-labeled high coverage, short linker SA-TMV particles (**2**) were incubated in lysosomal extract at pH 5 or PBS at pH 5 (hydrochloric acid was used to adjust the pH) at a concentration of 1 mg/mL. Samples were incubated at 37°C under gentle agitation and aliquots were taken at 6, 24, and 48 hrs and characterized by SDS-PAGE.

Results and discussion

Synthesis and characterization of SA-TMV constructs

TMV T158K mutant (TMV-lys)[17] was propagated and purified from *Nicotiana benthamiana* plants. A multistep protocol was used to produce a set of SA-TMV formulations (Fig. 1). TMV-lys was incubated with maleimide (MAL) and *N*-hydroxysuccinimide (NHS) dually-functionalized PEG_4 or PEG_{24} linkers (MAL-$PEG_{4/24}$-NHS). For high coverage particles, 10 equivalents of MAL-$PEG_{4/24}$-NHS were reacted per TMV-lys CP. For low coverage particles, 3 equivalents of MAL-$PEG_{4/24}$-NHS were reacted per TMV-lys CP. Four resulting PEG-TMVs were produced: low coverage MAL-PEG_4-TMV (**1′**), high coverage MAL-PEG_4-TMV (**2′**), low coverage MAL-PEG_{24}-TMV (**3′**), and high coverage MAL-PEG_{24}-TMV (**4′**). SA was reacted with NHS-PEG_4-SH separately to produce thiol-activated SA-

PEG_4-SH. The products from these two reactions were then combined to react via Michael addition to form SA-PEG_8-TMV or SA-PEG_{28}-TMV. To produce low coverage particles, 2 equivalents of SA-PEG_4-SH were reacted with **1′** or **2′**. To produce high coverage particles, 6 equivalents of SA-PEG_4-SH were reacted with **3′** or **4′**. Four SA-TMV constructs were produced: particles with low SA coverage and a short 8-mer PEG linker (**1**), particles with high SA coverage and short linker (**2**), particles with low SA coverage and a long 28-mer PEG linker (**3**), and particles with high SA coverage and a long PEG linker (**4**), as depicted in Fig. 1. Comparison between the resulting constructs allows for understanding the structure-function relationship guiding shielding of nanoparticles with SA, based on linker length and coverage density.

For each construct, the fully extended and average PEG linker length, as determined by Flory dimension (R_F), were calculated and are reported in Table 1.[5] R_F is an estimation of the hydrodynamic radius of the PEG linker, calculated for PEG based on the length of a monomer (0.35 nm for PEG)[5] and total number of monomers in the PEG chain (8 for constructs **1** and **2**, 28 for constructs **3** and **4**). The R_F was doubled to estimate the average PEG linker length.

Conjugation and structural integrity of the SA-TMV formulations were confirmed by SDS-polyacrylamide gel electrophoresis (SDS-PAGE; Fig. 2A), western blot analysis (WB; Fig. 2B), and negative stain transmission electron microscopy (TEM; Fig. 2C). The SDS-PAGE gel confirms the production of SA-TMV-lys coat protein (CP) conjugates of estimated molecular weight 83.5 kDa and above, corresponding to linked TMV-lys CP (17 kDa) and SA (66.5 kDa) (Fig. 2A). As expected, these higher molecular weight bands are not present in the TMV-lys and SA controls. The multiple band pattern of the SA-TMV conjugate may be explained by the fact that SA has multiple surface-exposed lysines available for conjugation with PEG; thus, individual SAs could display multiple PEG linkers. This could lead to polydisperse samples in which one SA may be conjugated to more than one neighboring TMV-lys CP simultaneously. Alternatively, modified CPs could engage through non-covalent interactions, as has been seen previously for other modified TMV formulations.[31, 32] The SDS-PAGE results are supported by WB probed with antibodies against TMV (Fig. 2B, pseudo-colored green) and against SA (Fig. 2B, pseudo-colored red). Overlaying the two WBs together confirms that TMV and SA are present in the same high molecular weight (SA-conjugated TMV CP) bands.

As expected, the SA-conjugated TMV CPbands on the SDS-PAGE gel are more intense for the high coverage particles (**2** and **4**) as compared to low coverage particles (**1** and **3**), indicating a higher degree of coverage. Using ImageJ and densitometry analysis of three SDS-PAGE gels corresponding to three distinct batches of SA-TMV particles, the average amount of SA per TMV was calculated for each formulation, as reported in Table 1. In preparing the particles, the ratios of SA to PEG-TMV were kept the same between high and low constructs, regardless of linker length (8× SA per TMV CP and 2× SA per TMV CP, respectively). However, there is approximately seven times more SA conjugation for **2** than **1** (the two short linker constructs), but only four times more SA conjugation for **4** than **3** (the two long linker constructs). Thus, the excess of reactive molecules is not the only limiting factor during conjugation. Furthermore, repeated conjugation experiments reveal that high

coverage particles prepared using the long linker show reduced SA conjugation, as compared to those prepared with the short linker. Specifically, **2**, which has approximately 300 SAs per TMV, has almost three times as much conjugated SA as **4**, which has approximately 110 SAs per TMV, despite using the same ratios of SA-PEG_4-SH to MAL-$PEG_{4/24}$-TMV. This could be because the long linker is more flexible and can adopt a tangled mushroom conformation, therefore its reactive end may not be surface exposed, leading to less overall conjugation (Fig. 2D). For low coverage particles, **1** and **3** have similar quantities of SA, with approximately 40 and 30 SAs per TMV, respectively.

In both the SDS-PAGE gel and WB, unconjugated TMV CPs and SA are present in the SA-TMV constructs (Fig. 2A, B). Free SA was present for all SA-TMV formulations, and has been reported previously for SA-TMV.[13] This is likely due to non-covalently attached SA that could be adsorbed to TMV or forming multimers with covalently attached SA. While we cannot rule out that some amount of the non-conjugated SA is free SA that is not associated with TMV, this is unlikely given the extensive washing steps and ultracentrifugation procedures employed during the purification steps.[13] The amount of free SA relative to the amount of TMV for each nanoparticle construct is as follows: 52.2 ± 14.4 μg/mg (**1**), 151.9 ± 44.8 μg/mg (**2**), 45.3 ± 22.5 μg/mg (**3**), and 94.4 ± 18.5 μg/mg (**4**). The amount of free SA for low coverage particles is similar to the amount of covalently-bound SA, supporting the possibility of SA dimerization. For the high coverage particles, the amount of free SA is less than the amount of conjugated SA, so it could be that not all SAs dimerize on the TMV surface or that the high coverage allows TMV-bound SAs to dimerize with one another. Regardless, these additional SA molecules could enhance camouflaging by sealing any gaps between covalently attached SAs on the TMV surface. For the long linker constructs, there is also an additional band of PEG_{24}-conjugated TMV CPs, with approximately 28.2 ± 0.7% of TMV CPs being PEGylated in **3** and 44.0 ± 5.5% of TMV CPs being PEGylated for **4**. This indicates that not all TMV CPs that are PEGylated are also conjugated with SA. Based on the PEG coverage and the R_F values reported in Table 1, we have determined that these PEGs likely adopt a mushroom conformation on the TMV surface.

TEM of the nanoparticles shows that all SA-TMV constructs remain intact after conjugation, and that the characteristic 300 nm by 18 nm rigid rod structure of TMV is preserved. Additionally, the high coverage particles **2** and **4** show the characteristic rough TMV surface (Fig. 2C); this is consistent with our previous TEM and structural studies.[28] It is apparent across the entire surface of **2**, while **4** appears rough in patches. The low coverage particles **1** and **3** do not have a rough TMV surface by TEM, likely because the SA coverage is not dense enough to markedly affect the appearance of the negative stain (Fig. 2C). The TEM images reveal some unconjugated SA aggregate, especially in construct **4**. This could be due to unconjugated SA getting tangled in the PEG mushrooms on the TMV surface during purification but being released when deposited on the TEM grids due to drying effects. This should not affect the analysis of these particles, however, because while tangled the SA should perform like conjugated protein in shielding the nanoparticle, and once dissociated from the TMV, the SA should act like free SA in the bloodstream.

Effects of SA coverage and linker length on shielding TMV

To determine the effectiveness of different SA coating strategies on immune recognition, dot blots using fluorescently-labeled TMV particles and TMV-specific antibodies were performed (Fig. 3A). To do so, nitrocellulose membranes were spotted in triplicate with 1 μL anti-TMV and 1 μL anti-cowpea mosaic virus (CPMV) antibody at 150 μg/mL. CPMV is an icosahedral plant virus and its antibodies act as a negative control. There are no structural similarities between CPMV and TMV and there is no cross-reactivity between the antibodies. After application of antibodies, membranes were blocked with 5% (w/v) milk, and then incubated with fluorescent Cy5-labeled nanoparticles. SA-TMV constructs (**1**-**4**) as well as the PEG-TMVs from which they were produced (**1′**-**4′**) were tested. After incubation with fluorescent SA-TMV and PEG-TMV particles, membranes were washed and dried, then imaged for fluorescence. If the particles interact with the antibodies, there would be a strong fluorescent signal where antibody-binding occurred.

Quantification of the dot blots indicates that for all cases, SA-TMV has reduced antibody recognition compared to its correlated PEG-TMV construct, as has been reported previously (Fig. 3B).[13, 28] We have also previously shown that both SA-TMV and PEG-TMV exhibit shielding properties and have significantly reduced binding compared to ‘naked’ TMV controls. Naked TMV samples were omitted in the data shown and we refer the reader to our previous paper.[13] Here, the SA-coated TMV particles display shielding effects from best to worst as follows: **2, 4 ⋙ 3 > 1 ⋙ 4′ ⋙> 2′ > 3′ ≫ 1′**. In all cases, when comparing particles with similar linker lengths high coverage was better, i.e. high coverage provides more efficient shielding and lower antibody recognition, compared to low coverage. Previous structural studies of SA-TMV indicated that SA shielding of TMV is, at least in part, due to steric hindrance preventing TMV-specific antibodies from reaching beyond the SA shield and also preventing tumbling of antibodies along the surface.[28] Therefore it seems logical that by lowering the number of shielding molecules on the TMV surface, there is more accessible area for epitope recognition, as well as antibody tumbling and binding.

Between PEG-TMV constructs, a longer PEG linker better shielded antibody recognition than a shorter linker in both cases, as has been reported previously for other plant viral nanoparticles.[5] For the SA-TMV constructs, the low coverage particles indicate that for similar SA coverage, a longer linker length is better (**3 > 1**). It is difficult to compare the high coverage particles, as **2** has approximately twice as much SA conjugated as **4**, but there is no significant difference in antibody recognition among high coverage particles. This suggests that perhaps there is a threshold for the amount of necessary shielding agents on the TMV surface.

To investigate the effects of the PEG linker on shielding, it is important to understand whether or not the PEG linker is surface-exposed, which could further prevent access to the TMV surface. To do so, dot blots were performed to assay the ability of PEG-specific antibodies to recognize the SA-TMV and PEG-TMV constructs (Fig. 3C, D). High coverage particles were chosen for this experiment, as previous dot blots indicated that the high coverage particles showed the best reduction in antibody recognition, regardless of linker length (Fig. 3A, B). While both the SA coatings on **2** and **4** provide protection from TMV-

specific antibodies, only the coating on **2** protects against PEG-specific antibodies. Thus, due to the exposed PEG linker on **4**, the particles must be shielded by both SA and PEG. Using the surface area of a TMV CP (8 nm^2) and the cross-section of SA (28-47 nm^2), it is estimated that 49-83% of the TMV nanoparticle surface is coated by SA for **2**.[28] In comparison, **4** has only 19-31% coverage. However, densitometry analysis indicates that 44% of TMV CPs are PEGylated in **4**. Using R_F to calculate the size of PEG in a mushroom conformation, we determined that the additional PEG could fully cover the remaining TMV surface for **4**. As both show successful protection against anti-TMV antibodies, this suggests that the 49-83% coverage provided by SA in **2** is sufficient for functional TMV camouflaging. Since **4** can be recognized by anti-PEG antibodies this limits use of this construct to clinical applications in which patients do not have pre-existing PEG antibodies. Overall, the *in vitro* antibody recognition data suggests that **2** would be the most clinically applicable construct.

Antibody response to multiple administrations of SA-TMV constructs

To address the immune response of differently coated SA-TMV nanoparticles *in vivo*, the antibody production of Balb/C mice in response to these particles was assessed. Mice (n = 3) were intravenously injected with either SA-TMV nanoparticles once per week for four weeks, mimicking a clinical setting in which patients may receive a weekly dosing with nanoparticles delivering chemotherapeutic regimen (Fig. 4A). Blood was drawn via retro-orbital bleed at days 0, 14, 28, and 56 to determine TMV-specific and SA-specific IgG antibody levels resulting from repeat administration. ELISA measurements using TMV or SA coated plates indicate that for all SA-TMV constructs, repeat administrations produce a robust antibody response to TMV but not to SA (Fig. 4B). This is critical for the clinical applicability of these particles moving forward, as an SA-specific antibody response would not only respond to the stealth coating on SA-TMV particles but could also respond to naturally occurring SA in the plasma.

To investigate the differences between TMV-specific IgG antibody titers in response to the different SA-TMV constructs, serial dilutions of plasma were analyzed by ELISA on TMV-coated plates (Fig. 4C). As expected, mice showed no preexisting TMV-specific IgG antibodies prior to the first treatment (day 0). At day 14 after two weeks of treatment, TMV and all SA-TMV constructs showed a similar TMV-reactive IgG response. More significant IgG levels were detected one week after the full treatment regimen at day 28, with all nanoparticles eliciting similar TMV-specific antibody responses. After the injections were stopped, mice retained circulating TMV-reactive IgGs, as seen on day 56. Taken together, the results from the ELISA experiments indicate that repeated administration of SA-camouflaged TMV nanoparticles leads to a robust anti-TMV immune response and this TMV-reactive IgG response occurs regardless of SA-coating formulation. Nevertheless, antibodies against the ‘self’ protein SA were not produced in the process, which indicates distinct processing of the TMV carrier vs. the SA coat.

Given the prevalence of TMV antibodies in the human population, in a clinical setting one would have to anticipate that a patient may already have TMV antibodies. Therefore, the key question is not whether anti-TMV antibodies are produced, but whether or not these anti-

TMV antibodies recognize the SA-TMV nanoparticle formulation. Accordingly, we investigated whether anti-TMV IgGs produced in response to repeat administration of SA-TMV would recognize the SA-TMV constructs. To do so, dot blots were performed with the diluted mouse plasma (1:200 dilution, one of the dilutions used for ELISA experiments in Fig. 4B) matched to the particles administered, *i.e.* plasma from the mice administered **1** would be tested against **1**, etc. As a control, mouse plasma from mice administered PBS were also tested against each construct. Unlike bare TMV particles, all SA-TMV constructs showed little antibody recognition (Fig. 5A). As shown for purified TMV-specific antibodies (see Fig. 3A, B), mouse plasma recognition was significantly reduced by SA coating (Fig. 5B).

Trafficking of SA-TMV nanoparticles upon cell uptake

Confocal microscopy was used to understand immune cell processing of the SA-TMV nanoparticles, after cell uptake in macrophages. Previous studies using flow cytometry indicate that SA-camouflage reduces, but does not completely eliminate, uptake of TMV into murine macrophages.[13] Since the antibody production experiments indicated that all formulations lead to the production of circulating anti-TMV antibodies but not anti-SA antibodies, we hypothesized that after nanoparticles are phagocytosed, SA and TMV undergo different fates. To test this, RAW 264.7 murine macrophage cells were incubated with **2**, as this construct was identified as the most effective at ‘stealthing’ TMV. A non-conjugated mixture of SA and TMV served as a control. A time course experiment was performed, in which particles were incubated with cells for 0, 6, 12, 24 hours, or 12 hours followed by washing and an additional 12 hours of incubation (Fig. 6A). After incubation, cells were fixed and stained with DAPI (blue), AlexaFluor 488-conjugated LAMP-1 to stain for lysosomes (red), or antibodies against TMV (green) and SA (cyan) with fluorescent secondary antibodies. The results show that SA-TMV enters macrophage cells and that TMV and the SA coating undergo different fates as was hypothesized. TMV appears within the lysosome by 12 hours and remains there until at least 24 hours after incubation (later time points were not tested). In contrast, SA appears to localize on the cell surface. For the control sample of SA mixed with TMV, TMV was detected within the lysosome by 6 hours and remained there for 24 hours. SA from the mixed sample is only weakly visualized in macrophages.

The discrepancy in the time before TMV is detected within the lysosome comparing SA-TMV vs. SA mixed with TMV is likely due to the shielding provided by the SA conjugation of the SA-TMV construct. Presumably the SA conjugation prevents TMV antibodies from binding and staining TMV until the 12 hour time point. By this point, the data indicates that the SA and TMV components of the construct have separated, thus allowing for staining of TMV in the lysosome. By 12 hours, SA is visualized at the periphery of the cell and remains there until at least 24 hours. As TMV is localized to the lysosome and SA is observed at the cell periphery there is no apparent colocalization of SA and TMV for the SA-TMV construct. This suggests that SA is cleaved and removed from the TMV carrier within the endolysosomal compartment and SA is recycled to the cell surface. While SA remains conjugated to TMV, the viral nanoparticle is shielded and not visualized as colocalized with

SA. Once SA is cleaved from SA-TMV, SA is likely trafficked away from the endolysosomal compartment.

To further investigate the fate of SA within macrophages, we compared the confocal results of the 12 hour incubation time point with that of 12 hours incubation followed by washing and an additional 12 hours of incubation (12 with 12 wash). The washing step is designed to remove any SA-TMV that has not already been taken up by the macrophages. For SA-TMV the results of the 12 with 12 wash condition indicate that the amount of SA is reduced compared to the 12 hour time point, suggesting either breakdown or cell export of SA during the 12 hours after the wash. In contrast, for SA mixed with TMV, there is never much intracellular signal for SA, suggesting that unconjugated SA is not as readily taken up by macrophages as the SA-TMV construct. This observation correlates with previous findings that SA is taken up more readily when in a multimeric form, likely due to having more attachment points to the membrane which prevents dissociation.[33]

The data presented in Fig. 6A suggests that SA may be cleaved from TMV between the 6 and 12 hour time points. To clarify the processing of the SA-TMV construct **2**, we investigated the colocalization of the SA, TMV, and the lysosome in more detail for time points of 6 hours (Fig. 6B, C) and 12 hours (Fig. 6D, E). Again, at the 6 hour time point little to no TMV is detected, but SA is detected, suggesting SA is still bound to the TMV surface and providing shielding. By measuring colocalization using the Mander's colocalization coefficient test, it appears that what little TMV is detectable is within the lysosome ($M = 0.62 \pm 0.12$), but does not colocalize with SA ($M = 0.25 \pm 0.12$). The Mander's colocalization coefficient also suggests that SA is not in the lysosome ($M = 0.37 \pm 0.07$). Therefore, SA could be trafficked from a different compartment, or could be cleaved from TMV before reaching the lysosome. Analyzing a z-stack cross-sectional view of a macrophage cell at 6 hours, puncta of SA are visualized within the cell but not colocalized with the lysosome (Fig. 6C).

By 12 hours, the TMV signal increased as described for Fig. 6A, suggesting SA has been cleaved by this time point (Fig. 6D). Mander's colocalization coefficient indicates again for the 12 hour time point that TMV is colocalized with the lysosome ($M = 0.80 \pm 0.08$) but less so with SA ($M = 0.49 \pm 0.05$). SA appears to be diffuse at the edges of the cell and could be at the cell membrane, as has been reported previously.[33] SA exhibits a low degree of lysosomal colocalization ($M = 0.50 \pm 0.03$). It appears that the colocalization between SA and TMV or SA and lysosomes only occurs when TMV and lysosomes are at the edges of the cell where SA is found, and it may not be true colocalization. This is supported further by a z-stack cross-sectional view of a macrophage cell at 12 hours, where TMV clearly colocalizes with the lysosome but SA remains on the edges of the cell, possibly at the cell membrane (Fig. 6E).

These results suggest that the conjugated nanoparticles are split into SA and TMV components after cell entry and traffic through different pathways. TMV travels to the lysosome, where it is likely degraded and processed, leading to presentation of TMV epitopes by antigen presenting cells and thereby stimulating the production of antibodies.[34] The results of the confocal microscopy experiments support the findings from the ELISA

experiments (Fig. 4C), where all SA-TMV constructs produced similar antibody responses. Presumably once the nanoparticles are taken up by immune cells, the cells process TMV similarly regardless of the construct. SA, on the other hand, appears to be exported from the cell, as it is found at the edges of the cell by 12 hours (Fig. 6D) and the amount of SA within the cell appears to be reduced after washing (Fig. 6A, 12 with 12 wash time point). Furthermore, the confocal microscopy results never indicate strong colocalization of SA with the lysosome, possibly because SA is trafficked out of the cell by SA receptors such as FcRn, gp60, gp18, and SPARC after entering cells but before reaching lysosomes.[35-41] FcRn has been previously reported to rescue SA from lysosomal degradation for recycling back to circulation, supporting this hypothesis.[42, 43]

SA-TMV cleavage and degradation in the lysosome

Endolysosomal proteasomes could be responsible for cleaving SA from TMV, allowing for SA recycling and TMV degradation, as seen by confocal microscopy. To determine if SA could be cleaved from TMV within the cell, Cy5-labeled SA-TMV construct **2** was incubated with lysosomal extract (LE) isolated from mouse livers at pH 5. As a control, nanoparticles were separately incubated at pH 5 in phosphate buffered saline (PBS) buffer. At 6 hours, 24 hours, and 48 hours, nanoparticles were extracted and run on SDS-PAGE. Gels were imaged for fluorescence (from the Cy5 label), then stained with Coomassie blue (Fig. 7A). By 48 hours, SA-TMV bands are absent from the gel but TMV CP monomer and dimer bands remain when **2** was incubated with LE (quantified in Fig. 7B). In contrast, when **2** was incubated in PBS at pH 5, all bands remain constant over time. This demonstrates that within the endolysosomal environment, SA can be cleaved from the TMV surface. While there is no increase in SA or TMV bands, it is likely that in the *ex vivo* experiments SA and TMV fragments may be further degraded. However *in vivo*, while TMV would remain in the lysosome, SA could be recycled by its receptors before degradation could occur.

Conclusions

This work highlights the utility of a bio-inspired camouflage, SA, for overcoming immune recognition of biologic-based nanoparticle delivery platforms. Our studies indicate that the effectiveness of SA shielding is dependent on the coverage characteristics, as has been reported previously for PEG shielding mechanisms.[5, 6] SA camouflage prevents antibody recognition (Fig. 8, step 1), with higher coverage leading to more effective shielding. Linker length also contributes to stealth properties, while formulations with longer linkers exhibit effective shielding; likely due to combinatory shielding effects from both SA and PEG; the SA-TMV formulations with longer linkers were recognized by anti-PEG antibodies. To avoid antibody recognition by anti-PEG antibodies, our data indicate, the best particles to develop for clinical translation are the particles with high SA coverage and short PEG linkers (construct **2**). While administration of SA-TMV particles *in vivo* results in production of TMV-specific antibodies, these anti-TMV antibodies do not recognize the SA-coated TMV nanoparticles (Fig 8, step 5). SA-specific antibodies are not produced, likely because TMV and SA follow distinct intracellular pathways, i.e. endolysosomal degradation of TMV and recycling of SA (Fig. 8, steps 2-4). Previous findings show that small chemical modifiers are cleaved rapidly from TMV particles when exposed to endolysosomal

conditions.[30] Here we show that even large cargoes, such as SA, are cleaved from the nanoparticles. These results also have implications for cargo delivery, where release in the endolysosome would be desired (e.g. cell permeable drugs or drugs acting on the endolysosome). TMV nanoparticles are already being explored as carriers for various drugs loaded into the central channel of the virus.[20, 44, 45] Future applications could involve loading hydrophobic drugs onto the SA component of an SA-TMV nanoparticle for a dual-delivery approach.

Acknowledgments

This work was supported in parts by a grant from NIH, R01-CA202814 (to N.F.S.). N.M.G. was supported in part by NIH T32 GMS008803. We thank Christina Wege and her team (University of Stuttgart) for providing TMV-lys.

References

1. Blanco E, Shen H, Ferrari M. Nat Biotechnol. 2015; 33:941–951. [PubMed: 26348965]
2. Lee YK, Choi EJ, Webster TJ, Kim SH, Khang D. Int J Nanomedicine. 2015; 10:97–113. [PubMed: 25565807]
3. Kokkinopoulou M, Simon J, Landfester K, Mailander V, Lieberwirth I. Nanoscale. 2017; 9:8858–8870. [PubMed: 28632260]
4. Walczyk D, Bombelli FB, Monopoli MP, Lynch I, Dawson KA. J Am Chem Soc. 2010; 132:5761–5768. [PubMed: 20356039]
5. Lee KL, Shukla S, Wu M, Ayat NR, El Sanadi CE, Wen AM, Edelbrock JF, Pokorski JK, Commandeur U, Dubyak GR, Steinmetz NF. Acta Biomater. 2015; 19:166–179. [PubMed: 25769228]
6. Perry JL, Reuter KG, Kai MP, Herlihy KP, Jones SW, Luft JC, Napier M, Bear JE, DeSimone JM. Nano letters. 2012; 12:5304–5310. [PubMed: 22920324]
7. Gref R, Luck M, Quellec P, Marchand M, Dellacherie E, Harnisch S, Blunk T, Muller RH. Colloids Surf B Biointerfaces. 2000; 18:301–313. [PubMed: 10915952]
8. Ganson NJ, Povsic TJ, Sullenger BA, Alexander JH, Zelenkofske SL, Sailstad JM, Rusconi CP, Hershfield MS. J Allergy Clin Immunol. 2016; 137:1610–1613 e1617. [PubMed: 26688515]
9. Garay RP, El-Gewely R, Armstrong JK, Garratty G, Richette P. Expert Opin Drug Deliv. 2012; 9:1319–1323. [PubMed: 22931049]
10. Ganson NJ, Kelly SJ, Scarlett E, Sundy JS, Hershfield MS. Arthritis Res Ther. 2006; 8:R12. [PubMed: 16356199]
11. Hershfield MS, Ganson NJ, Kelly SJ, Scarlett EL, Jaggers DA, Sundy JS. Arthritis Res Ther. 2014; 16:R63. [PubMed: 24602182]
12. Rodriguez PL, Harada T, Christian DA, Pantano DA, Tsai RK, Discher DE. Science. 2013; 339:971–975. [PubMed: 23430657]
13. Pitek AS, Jameson SA, Veliz FA, Shukla S, Steinmetz NF. Biomaterials. 2016; 89:89–97. [PubMed: 26950168]
14. Mariam J, Sivakami S, Dongre PM. Drug Deliv. 2016; 23:2668–2676. [PubMed: 26056719]
15. Bruckman MA, Randolph LN, VanMeter A, Hern S, Shoffstall AJ, Taurog RE, Steinmetz NF. Virology. 2014; 449:163–173. [PubMed: 24418549]
16. Bruckman MA, Steinmetz NF. Methods in molecular biology. 2014; 1108:173–185. [PubMed: 24243249]
17. Geiger FC, Eber FJ, Eiben S, Mueller A, Jeske H, Spatz JP, Wege C. Nanoscale. 2013; 5:3808–3816. [PubMed: 23519401]
18. Bruckman MA, Randolph LN, Gulati NM, Stewart PL, Steinmetz NF. J Mater Chem B Mater Biol Med. 2015; 3:7503–7510. [PubMed: 26659591]
19. Bruckman MA, Jiang K, Simpson EJ, Randolph LN, Luyt LG, Yu X, Steinmetz NF. Nano Lett. 2014; 14:1551–1558. [PubMed: 24499194]

20. Czapar AE, Zheng YR, Riddell IA, Shukla S, Awuah SG, Lippard SJ, Steinmetz NF. ACS Nano. 2016; 10:4119–4126. [PubMed: 26982250]
21. Sakata Y, Chen YY, Chen HR, Zhao JH, Xu QX. J Jpn Soc Hortic Sci. 1997; 66:99–104.
22. Cai WQ, Fang RX, Shang HS, Wang X, Zhang FL, Li YR, Zhang JC, Cheng XY, Wang GL, Mang KQ. Mol Breeding. 2003; 11:25–35.
23. Pinnow DL, Demski JW, Sterling J. Georgia Agr Res. 1981; 22:6–6.
24. Asselin A. Phytoprotection. 1979; 60:170–171.
25. Gottula J, Fuchs M. Adv Virus Res. 2009; 75:161–183. [PubMed: 20109666]
26. Balique F, Colson P, Raoult D. J Clin Virol. 2012; 55:374–376. [PubMed: 22959216]
27. Liu R, Vaishnav RA, Roberts AM, Friedland RP. PLoS One. 2013; 8:e60621. [PubMed: 23573274]
28. Gulati NM, Pitek AS, Steinmetz NF, Stewart PL. Nanoscale. 2017; doi: 10.1039/c6nr06948g
29. Schneider CA, Rasband WS, Eliceiri KW. Nat Methods. 2012; 9:671–675. [PubMed: 22930834]
30. Wen AM, Infusino M, De Luca A, Kernan DL, Czapar AE, Strangi G, Steinmetz NF. Bioconjug Chem. 2015; 26:51–62. [PubMed: 25541212]
31. Altintoprak K, Seidenstucker A, Welle A, Eiben S, Atanasova P, Stitz N, Plettl A, Bill J, Gliemann H, Jeske H, Rothenstein D, Geiger F, Wege C. Beilstein J Nanotechnol. 2015; 6:1399–1412. [PubMed: 26199844]
32. Bruckman MA, VanMeter A, Steinmetz NF. ACS Biomater Sci Eng. 2015; 1:13–18. [PubMed: 25984569]
33. Schmidtke JR, Unanue ER. J Immunol. 1971; 107:331–338. [PubMed: 5568765]
34. Watts C. Biochim Biophys Acta. 2012; 1824:14–21. [PubMed: 21782984]
35. Anderson CL, Chaudhury C, Kim J, Bronson CL, Wani MA, Mohanty S. Trends Immunol. 2006; 27:343–348. [PubMed: 16731041]
36. Chaudhury C, Mehnaz S, Robinson JM, Hayton WL, Pearl DK, Roopenian DC, Anderson CL. J Exp Med. 2003; 197:315–322. [PubMed: 12566415]
37. Schnitzer JE, Bravo J. J Biol Chem. 1993; 268:7562–7570. [PubMed: 8463286]
38. Schnitzer JE, Oh P. J Biol Chem. 1994; 269:6072–6082. [PubMed: 8119952]
39. Merlot AM, Kalinowski DS, Richardson DR. Front Physiol. 2014; 5:299. [PubMed: 25161624]
40. Schnitzer JE. Am J Physiol. 1992; 262:H246–254. [PubMed: 1733316]
41. Schnitzer JE, Oh P. Am J Physiol. 1992; 263:H1872–1879. [PubMed: 1481911]
42. Kim J, Bronson CL, Hayton WL, Radmacher MD, Roopenian DC, Robinson JM, Anderson CL. Am J Physiol Gastrointest Liver Physiol. 2006; 290:G352–360. [PubMed: 16210471]
43. Sarav M, Wang Y, Hack BK, Chang A, Jensen M, Bao L, Quigg RJ. J Am Soc Nephrol. 2009; 20:1941–1952. [PubMed: 19661163]
44. Lee KL, Carpenter BL, Wen AM, Ghiladi RA, Steinmetz NF. ACS Biomater Sci Eng. 2016; 2:838–844. [PubMed: 28713855]
45. Chariou PL, Steinmetz NF. ACS Nano. 2017; 11:4719–4730. [PubMed: 28345874]

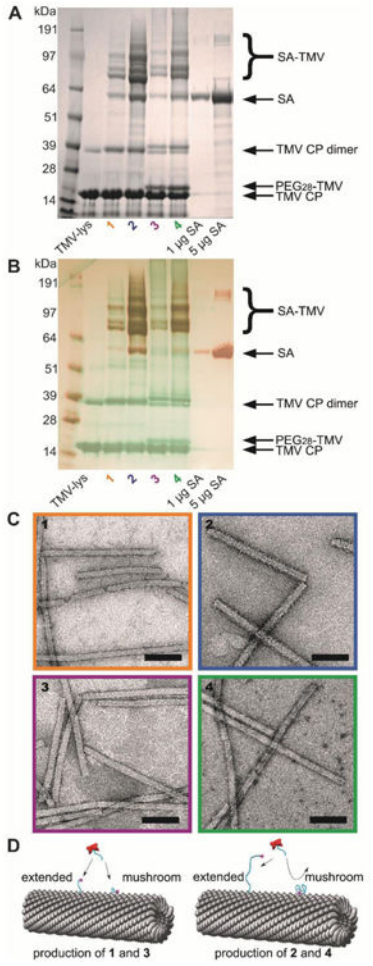

Fig. 1.

Cartoon depiction of production of four PEG-TMV and four SA-TMV constructs, with varying PEG linker length and SA coverage quantity. TMV shown in gray, PEG linker shown in cyan, and serum albumin shown in red. Conjugation of PEG_4 or PEG_{24} to TMV results in four PEG-TMV constructs: **1′** (short linker, low coverage), **2′** (short linker, high coverage), **3′** (long linker, low coverage), and **4′** (long linker, high coverage). PEG-TMV constructs are reacted with PEG_4-conjugated SA to yield four SA-TMV constructs: **1** (short linker, low coverage) as shown in the orange box, **2** (short linker, high coverage) in the blue box, **3** (long linker, low coverage) in the purple box, and **4** (long linker, high coverage) in the green box.

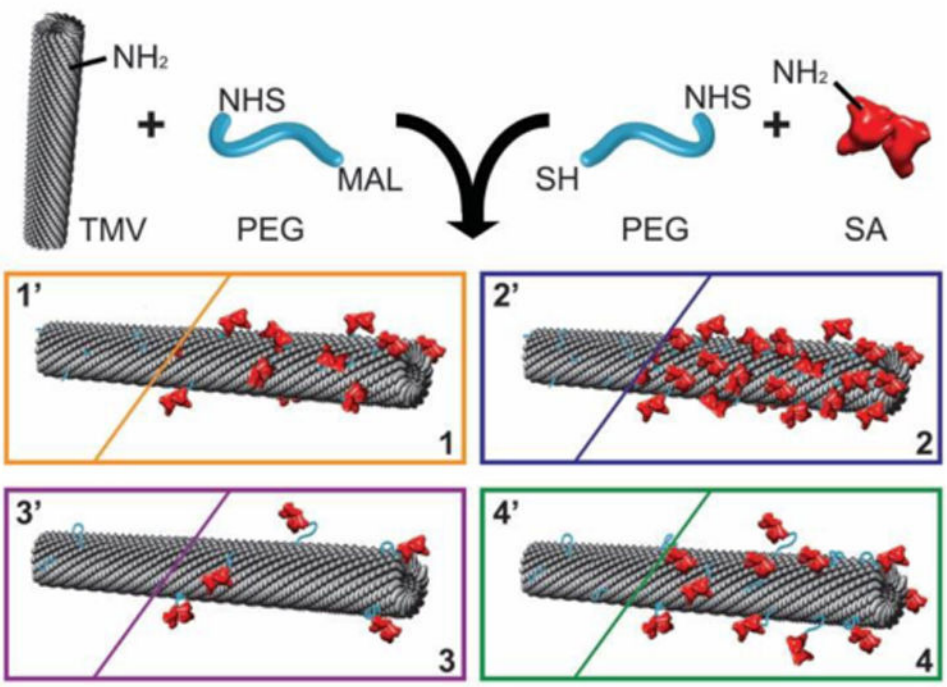

Fig. 2.

Characterization of SA-TMV constructs. A) Representative SDS-PAGE gel. B) Overlaid WBs against TMV (green) and SA (red). C) Negative stain TEM micrographs showing intact SA-TMV particles. The four SA-TMV constructs are: **1** (short linker, low coverage), **2** (short linker, high coverage), **3** (long linker, low coverage), and **4** (long linker, high coverage). Scale bars = 100 nm. D) Schematic showing SA interacting with PEGs on TMV, with the mushroom conformation of 24-mer PEG preventing conjugation. Reactive end denoted with a star.

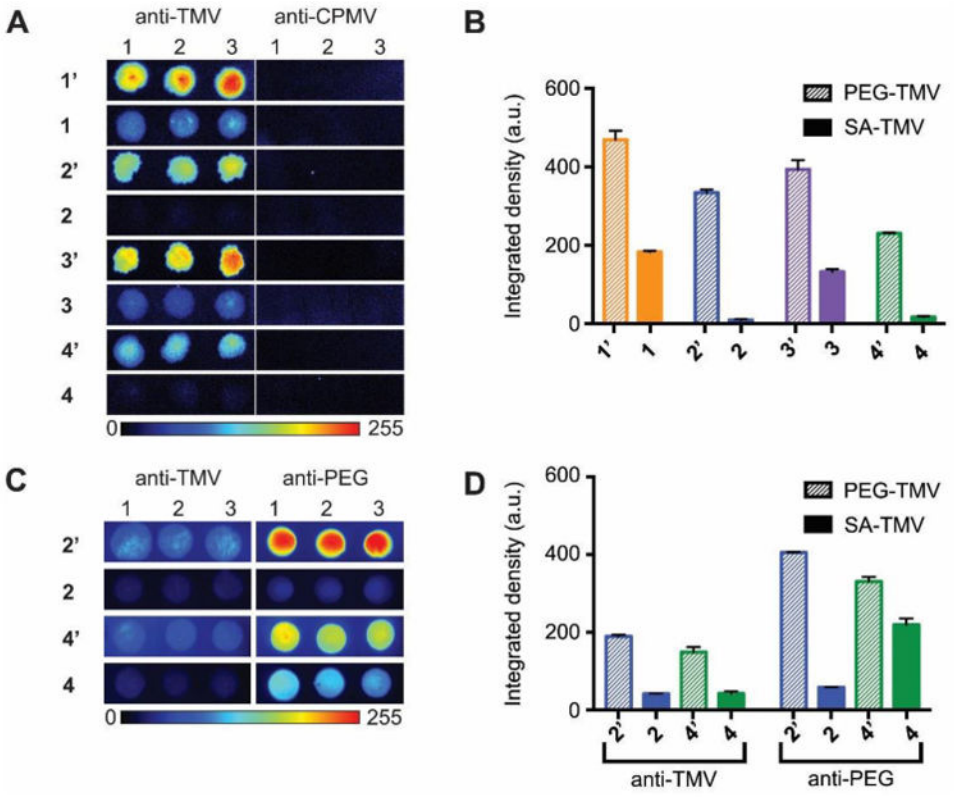

Fig. 3.

Antibody recognition of SA-TMV and PEG-TMV constructs. A) Dot blots of anti-TMV or anti-CPMV recognition of fluorescent SA-TMV constructs (**1**-**4**) and their corresponding PEG-TMV control constructs (**1′**-**4′**). B) Densitometry quantification of fluorescent TMV signal corresponding to antibody recognition by anti-TMV antibodies from A. C) Dot blots of anti-TMV or anti-PEG recognition of fluorescent high coverage SA-TMV constructs (**2** and **4**) and their corresponding PEG-TMV control constructs (**2′** and **4′**). D) Densitometry quantification of fluorescent TMV signal corresponding to antibody recognition by anti-TMV and anti-PEG antibodies from C.

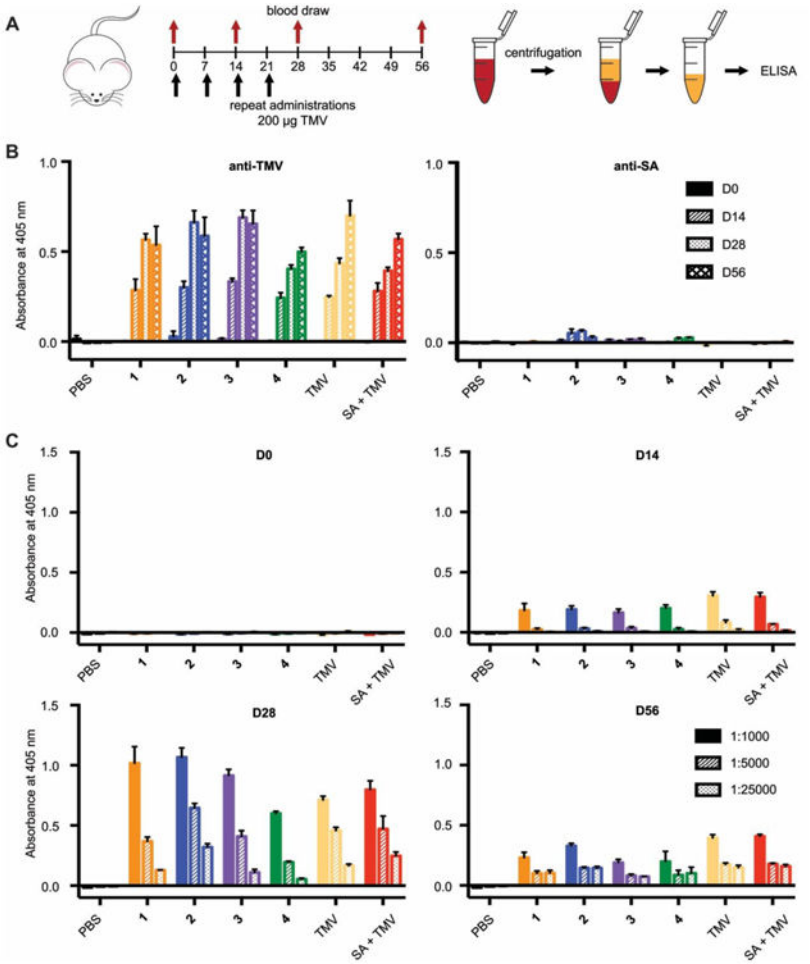

Fig. 4.

Quantification of antibodies generated after repeated administration of SA-TMV constructs. A) Schematic of multiple administration and bleeding schedules (left); preparation of blood plasma and analysis by ELISA (right). B) ELISA results showing production of TMV-specific but not SA-specific antibodies. C) ELISA results showing increasing levels of TMV-specific antibodies after multiple administrations.

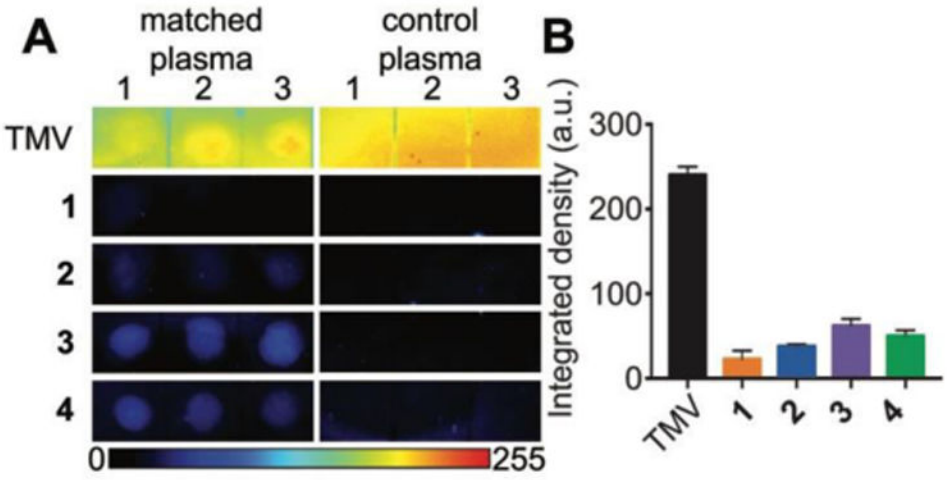

Fig. 5.

Analysis of SA-TMV recognition by antibodies in plasma from immunized mice. A) Dot blots indicating recognition of SA-TMV constructs by antibodies in 1:200 diluted plasma from immunized mice. B) Densitometry quantification of fluorescent TMV signal from A corresponding to recognition by anti-TMV antibodies in diluted plasma.

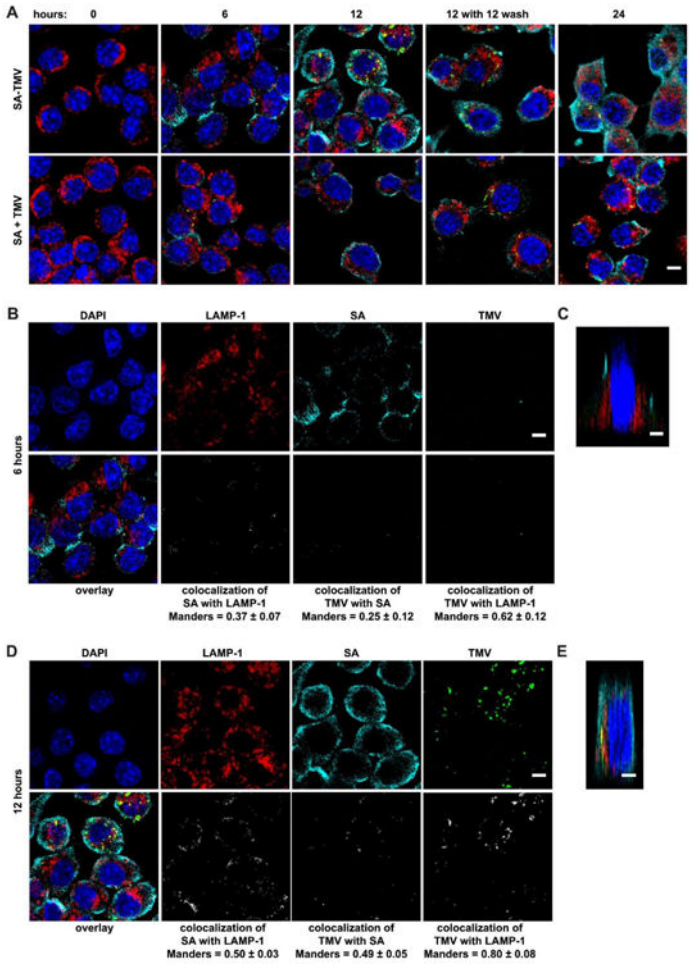

Fig. 6.

Confocal microscopy of SA-TMV uptake by RAW 264.7 murine macrophage cells. A) Uptake time course of SA-conjugated TMV or mixed SA and TMV (SA+TMV). SA labeled in cyan, TMV in green, lysosome LAMP-1 marker in red, and nucleus (DAPI) in blue. B) Colocalization analysis of the intracellular distribution of SA-TMV in RAW 264.7 cells at 6 hour time point. C) Z-stack cross-section of RAW 264.7 cell exposed to SA-TMV at 6 hour time point. D) Colocalization analysis of the intracellular distribution of SA-TMV in RAW 264.7 cells at 12 hour time point. E) Z-stack cross-section of RAW 264.7 cell exposed to SA-TMV at 12 hour time point. Scale bars = 5 μm.

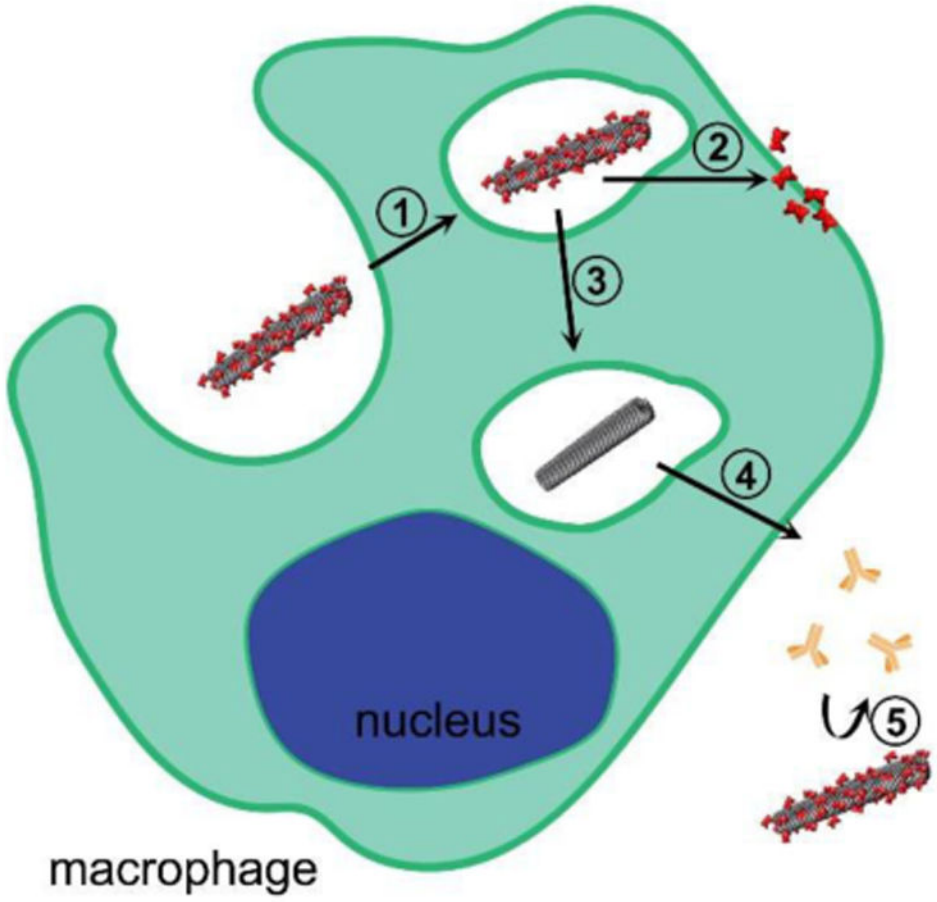

Fig. 7.

Schematic of SA-TMV nanoparticle fate *in vivo*. Nanoparticles are phagocytosed by immune cells such as macrophages (step 1). From there, SA is cleaved from the TMV surface and can be exported out of the cell (step 2). TMV is trafficked towards the lysosome (step 3), where it is degraded leading to antibody production (step 4). However, produced antibodies are unable to recognize SA-shielded nanoparticles (step 5).

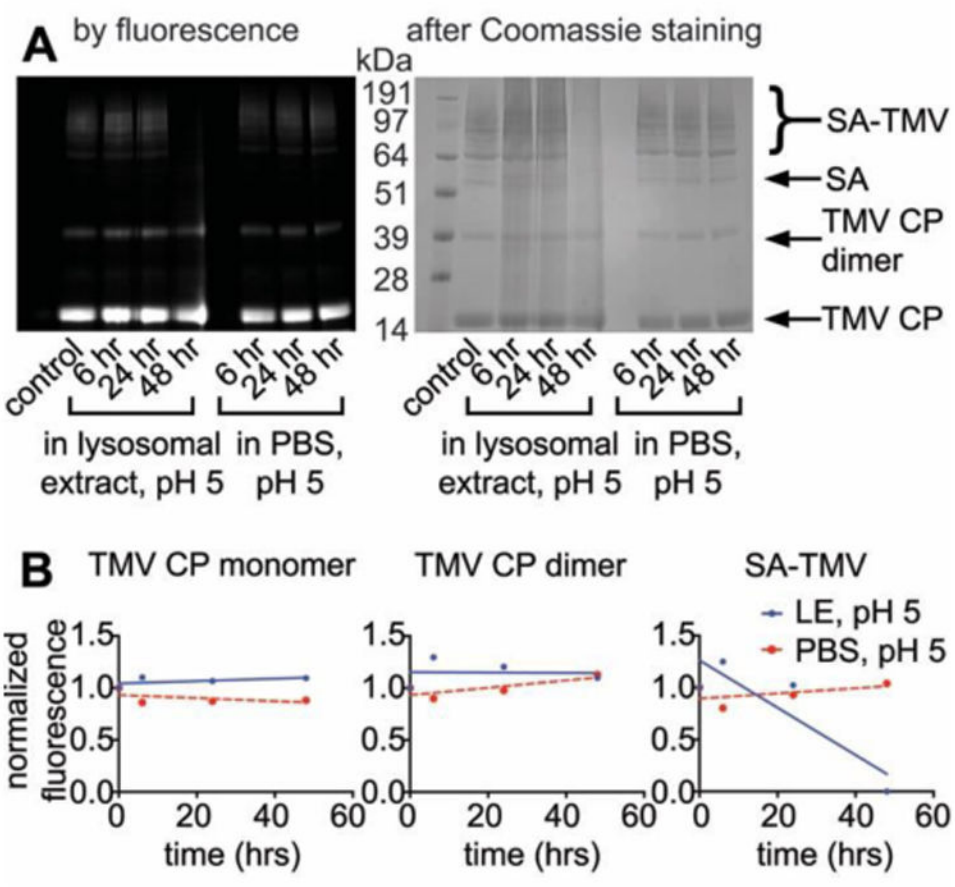

Fig. 8.

Stability of Cy5-labeled SA-TMV in lysosomal extract (LE) over time. A) SDS-PAGE results over time, imaged first by fluorescence (left), then stained with Coomassie blue and imaged by white light (right). B) Densitometry quantification of fluorescent band intensity for TMV CP monomer (left), TMV CP dimer (middle), and sum of SA-TMV bands (right).

Table 1

Physical characteristics of SA coverage and PEG linkers of SA-TMV constructs.

SA-TMV construct	Number of PEG monomers	PEG molecular weight (Da)	Average PEG diameter (nm)[a]	Fully extended PEG length (nm)[b]	SA concentration (μg SA / mg TMV)[c]	# SAs per TMV[d]	TMV surface coverage by SA[e]
1	8	363	2.44	2.8	78.4 ± 23.1	44 ±13	7-12%
2	8	363	2.44	2.8	534.9 ± 146.8	301 ± 83	49-83%
3	28	1275	5.17	9.8	53.0 ± 20.3	30 ± 12	5-8%
4	28	1275	5.17	9.8	202.6 ±108.5	114 ± 61	19-31%

[a]Determined by doubling RF of each PEG construct to get diameter length.;

[b]Calculated by multiplying the number of PEG monomers by the length of a single monomer (0.35 nm);

[c]Estimated by densitometry analysis of bands with molecular weight >64 kDa from three SDS-PAGE gels of different batches of SA-TMV constructs;

[d]Calculated using the SA concentration based on three SDS-PAGE gels and the molecular weights of SA and TMV;

[e]Calculated using the number of SAs per TMV and the cross-sectional area of SA (28-47 nm^2) compared to the approximate surface area of TMV (17,040 nm^2).